A PARTITION-OF-UNITY METHOD FOR MODELING COUPLED THERMO-MECHANICAL PROBLEMS IN FRP LAMINATES SUBJECTED TO IMPACT

A. Ahmed[1,2*] , L.J. Sluys[1]

[1]Faculty of Civil Engineering and Geosciences, Delft University of Technology, Delft, Netherlands

[2]Department of Civil Engineering, N-W.F.P University of Engineering & Technology, Peshawar, Pakistan

*Corresponding author (A.Ahmed@tudelft.nl)

Keywords: *Thermo-mechanics, adiabatic/isothermal cracking, Finite element method, Partition-of-unity, Impact*

1 Introduction

In many engineering applications fiber-reinforced composite structures are often subjected to extreme loading conditions such as impact, thermal shock, thermal cycles etc. In the event of impact loading, the energy which is in excess of the energy required for the creation of new crack surfaces, is dissipated as heat. This may result in a substantial increase in local temperature near the crack tip region. This internal heat generation process can significantly influence the mechanical response of the material and results in further degradation of material strength and stiffness [1]. Moreover, presence of cracks in a solid hinder the flow of temperature within the solid, consequently affecting the temperature profile and thermal strains. As a result the composite response may be affected significantly.

In the experimental study of [2,3], graphite-epoxy unidirectional laminates were subjected to impact. The formation of localized heated zones were observed near the crack surfaces. The temperature rise was about 70^oC and was attributed to frictional sliding of the crack faces. Similar impact tests were performed on brittle polymers by [4] and it was observed that the localized increase of temperature in crack-tip region, due to dissipative processes during fracture, influenced the energy release rate of the crack and consequently, the crack propagation speed. Numerical analysis of such coupled multi-physics problems including crack growth, requires the use of efficient and reliable computational tools, which are able to capture the rate effects and predict the strength of composites.

The aim of this study is to present a comprehensive coupled thermo-mechanical finite element model for the analysis of damage growth in fiber-reinforced laminated composite plates subjected to impact. This is achieved through a coupled equation of motion and energy equation accounting for the effects of cohesive interfaces, inertia and heat conduction. In order to properly model different fracture modes and their interaction, a discrete fracture approach is used to model damage processes such as inter-laminar and intra-laminar damage in fiber-reinforced laminated composites. Moreover, the presence of inter- and/or intra-laminar cracks in a laminate causes obstructions in the flow of heat and thus results in a discontinuous heat flow across the crack. This behavior is also modeled using a discontinuous finite element approach.

One of the preferred computational paradigms to model mesh independent discontinuities within the framework of finite element method, is the Partition-of-unity approach [5]. In the present work, the Partition-of-unity approach is exploited not only to model discontinuities in the displacement field but

also to model discontinuities in the temperature and heat flux fields. As a consequence, it is possible to simulate both adiabatic as well as isothermal cracks, propagating independently of the finite element mesh. This is achieved within the framework of the phantom node method [6], which results in an efficient and robust finite element implementation.

2 Thermo-mechanical discrete damage model

2.1 Balance of linear momentum

Consider a body with domain Ω crossed by an internal boundary (crack) Γ_c with unit normal $\mathbf{n}_c$, figure 1. The balance of linear momentum in the current configuration is given as

$$\int_{\Omega} (\nabla \cdot \boldsymbol{\sigma} + \mathbf{b}) = \mathbf{0} \tag{1}$$

in which $\boldsymbol{\sigma}$ is the Cauchy stress tensor, $\mathbf{b}$ is the body force and ∇ is the gradient with respect to current configuration.

To simulate mesh independent matrix cracking/splitting in individual plies of the laminate, the phantom node method [6] is exploited. The idea is to replace the cracked element, with domain Ω^{elem}, with a pair of partially active overlapping elements with domains Ω_A^{elem} and Ω_B^{elem}, respectively, such that $\Omega^{elem} = \Omega_A^{elem} \cup \Omega_B^{elem}$. The superscript $elem$ represents a particular element in a finite element mesh crossed by a discontinuity.

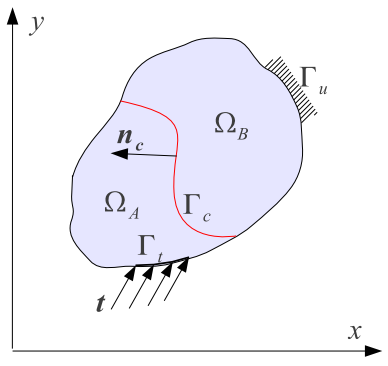

Fig. 1. Body $\Omega = \Omega_A \cup \Omega_B$ crossed by a crack Γ_c

The displacement field $\mathbf{u}$ of a cracked element is given as

$$\mathbf{u}(\mathbf{x}) = \begin{cases} \mathbf{u}_A(\mathbf{x}) & \forall \mathbf{x} \in \Omega_A \\ \mathbf{u}_B(\mathbf{x}) & \forall \mathbf{x} \in \Omega_B \end{cases} \tag{2}$$

The displacement jump $[\![\mathbf{u}]\!]$ over the crack is defined as the difference of the displacement fields of the two elements

$$[\![\mathbf{u}]\!](\mathbf{x}) = \mathbf{u}_A(\mathbf{x}) - \mathbf{u}_B(\mathbf{x}) \qquad \forall \mathbf{x} \in \Gamma_c \tag{3}$$

At the crack, the continuity condition $\mathbf{t}_{c/A} = -\mathbf{t}_{c/B} = -\mathbf{t}_c$ has to be satisfied. Moreover, under the assumption of small deformations at the interface, the unit normal at the interface can be uniquely defined as $\mathbf{n}_{c/A} = -\mathbf{n}_{c/B} = -\mathbf{n}_c$.

By applying a standard Galerkin procedure to equation (1), the following weak form of balance of linear momentum is obtained

$$\int_{\Omega_A} \rho \delta \mathbf{u}_A \cdot \ddot{\mathbf{u}}_A + \int_{\Omega_A} \delta \boldsymbol{\epsilon}_A : \boldsymbol{\sigma}_A + \int_{\Gamma_c} \delta \mathbf{u}_A \cdot \mathbf{t}_c - \int_{\Gamma_{t,A}} \delta \mathbf{u}_A \cdot \mathbf{t} - \int_{\Omega_A} \delta \mathbf{u}_A \cdot \mathbf{b} = \mathbf{0} \tag{4a}$$

$$\int_{\Omega_B} \rho \delta \mathbf{u}_B \cdot \ddot{\mathbf{u}}_B + \int_{\Omega_B} \delta \boldsymbol{\epsilon}_B : \boldsymbol{\sigma}_B + \int_{\Gamma_c} -\delta \mathbf{u}_B \cdot \mathbf{t}_c - \int_{\Gamma_{t,B}} \delta \mathbf{u}_B \cdot \mathbf{t} - \int_{\Omega_B} \delta \mathbf{u}_B \cdot \mathbf{b} = \mathbf{0} \tag{4b}$$

2.2 Balance of energy

The energy balance for material exhibiting plasticity is given as

$$\int_{\Omega} \rho C_p \dot{\theta} - \int_{\Omega} \boldsymbol{\sigma} \cdot \dot{\boldsymbol{\epsilon}}_p - \int_{\Omega} \rho s + \int_{\Omega} \nabla \mathbf{q} = \mathbf{0} \tag{5}$$

in which θ is the temperature field, C_p is the specific heat, $\dot{\boldsymbol{\epsilon}}_p$ is the plastic strain rate due to fibre failure, ρ is the current density, s is the heat power per unit mass and $\mathbf{q}$ is the heat flux. In the above equation, it is considered that the thermo-elastic contribution on the internal work is small and a major part of the plastic work, due to fibre failure and/or other failure mechanisms such as shear nonlinearity, is converted into heat.

The temperature field in a cracked element is defined as [7]

$$\theta(\mathbf{x}) = \begin{cases} \theta_A(\mathbf{x}) & \forall \mathbf{x} \in \Omega_A \\ \theta_B(\mathbf{x}) & \forall \mathbf{x} \in \Omega_B \\ \theta_c(\mathbf{x}) & \forall \mathbf{x} \in \Gamma_c \end{cases} \tag{6}$$

Note that, independent definitions of the temperature field on both sides of the crack allows to model a discontinuity in the temperature field across the crack surface. After applying the weighted test function $\delta\theta$, the weak form of energy equation takes the form

$$\int_\Omega \delta\theta \rho C_p \dot{\theta} - \int_\Omega \delta\theta(\boldsymbol{\sigma} \cdot \dot{\boldsymbol{\epsilon}}_p) - \int_\Omega \rho \delta\theta s + \int_\Omega \delta\theta \nabla \mathbf{q} = \mathbf{0} \tag{7}$$

In particular, the divergence term in equation (7) can be expanded by means of integration by parts and applying the divergence theorem

$$\int_\Omega \delta\theta \nabla \mathbf{q} = -\int_\Omega \nabla\delta\theta : \mathbf{q} + \int_{\Gamma_q} \delta\theta(\mathbf{n} \cdot \mathbf{q}) + \int_{\Gamma_c^A} \delta\theta_A(\mathbf{n}_A \cdot \mathbf{q}_A) + \int_{\Gamma_c^B} \delta\theta_B(\mathbf{n}_B \cdot \mathbf{q}_B) \tag{8}$$

$$= -\int_\Omega \nabla\delta\theta : \mathbf{q} + \int_{\Gamma_q} \delta\theta Q + \int_{\Gamma_c^A} \delta\theta_A Q_A + \int_{\Gamma_c^B} \delta\theta_B Q_B \tag{9}$$

Γ_c^A and Γ_c^B are the crack surfaces corresponding to domains Ω_A and Ω_B, respectively. Substituting equation (9) in equation (7) and then exploiting the additive property of integrals, equation (7) can be written as two independent energy balance equations for the domains Ω_A and Ω_B as

$$\int_{\Omega_A} \delta\theta_A \rho C_p \dot{\theta} - \int_{\Omega_A} \delta\theta_A(\boldsymbol{\sigma} \cdot \dot{\boldsymbol{\epsilon}}_{p/A}) - \int_{\Omega_A} \nabla\delta\theta_A : \mathbf{q} + \int_{\Gamma_c^A} \delta\theta_A Q_A - \int_{\Omega_A} \delta\theta_A \rho s + \int_{\Gamma_q^A} \delta\theta_A Q = \mathbf{0} \tag{10}$$

$$\int_{\Omega_B} \delta\theta_B \rho C_p \dot{\theta} - \int_{\Omega_B} \delta\theta_B(\boldsymbol{\sigma} \cdot \dot{\boldsymbol{\epsilon}}_{p/B}) - \int_{\Omega_B} \nabla\delta\theta_B : \mathbf{q} + \int_{\Gamma_c^B} \delta\theta_B Q_B - \int_{\Omega_B} \delta\theta_B \rho s + \int_{\Gamma_q^B} \delta\theta_B Q = \mathbf{0} \tag{11}$$

Note that we do not enforce the continuity of flux across the crack surface, i.e

$$Q_A \neq -Q_B \tag{12}$$

which otherwise would have been resulted in a formulation similar to [8]. As a result of non-enforcement of continuity of heat flux at the interface and by the virtue of defining an interface temperature θ_c (equation 6), it is possible to model a discontinuity in the heat flux field in addition to the discontinuity in the temperature field.

The heat flux through an interface is defined as

$$Q_A = -k_c \left(\frac{\partial \theta_A}{\partial n_c} \right)_{\Gamma_c^A} = -k_c(\theta_c - \theta_A) \tag{13a}$$

$$Q_B = -k_c \left(\frac{\partial \theta_B}{\partial n_c} \right)_{\Gamma_c^B} = -k_c(\theta_c - \theta_B) \tag{13b}$$

in which k_c is the interface conductance coefficient. The explicit form of k_c depends upon the effect of the crack bridging, damage at the interface, displacement jump, crack surface roughness etc. For more details, see for example [8].

The interface temperature, θ_c, can be obtained through the assumption of energy balance at the interface and is given as

$$\theta_c = \frac{\mathbf{t} \cdot [\![\dot{\mathbf{u}}]\!]}{2k_c} + \frac{\theta_A + \theta_B}{2} \tag{14}$$

Note that, the first term in equation (14) is responsible for heat generation at the interface due to interface dissipation.

3 Constitute equations

The bulk material response is considered to be linear elastic. The stress-strain relation is given as

$$\boldsymbol{\sigma} = \mathbb{C} : (\boldsymbol{\epsilon} - \boldsymbol{\epsilon}_\theta) \tag{15}$$

in which $\mathbb{C}$ is the fourth-order material tangent stiffness tensor with

$$[\mathbf{C}]^{-1} = \begin{bmatrix} \frac{1}{E_1} & \frac{-\nu_{21}}{E_2} & \frac{-\nu_{31}}{E_3} & 0 & 0 & 0 \\ \frac{-\nu_{12}}{E_1} & \frac{1}{E_2} & \frac{-\nu_{32}}{E_3} & 0 & 0 & 0 \\ \frac{\nu_{13}}{E_1} & \frac{-\nu_{23}}{E_2} & \frac{1}{E_3} & 0 & 0 & 0 \\ 0 & 0 & 0 & \frac{1}{G_{12}} & 0 & 0 \\ 0 & 0 & 0 & 0 & \frac{1}{G_{23}} & 0 \\ 0 & 0 & 0 & 0 & 0 & \frac{1}{G_{13}} \end{bmatrix} \tag{16}$$

in which $\mathbf{C}$ is the matrix form of tensor $\mathbb{C}$, obtained using Voigt notation. The subscripts 1,2 and 3 denote the orthogonal axes of the principal material coordinate system. $\boldsymbol{\epsilon}_\theta$ is the thermal strain tensor and is considered to be purely volumetric. The thermal strain tensor in Voigt notation is given as

$$\{\boldsymbol{\epsilon}_\theta\} = \{\alpha_1\theta, \alpha_2\theta, \alpha_3\theta, 0, 0, 0\}^T \tag{17}$$

in which α_1, α_2 and α_3 are linear coefficients of thermal expansion in material principle directions.

The constitutive assumption for heat conduction is given by Fourier′s law as

$$\mathbf{q} = -\mathbf{k}\nabla\theta \tag{18}$$

in which the matrix $\mathbf{k}$ is the conductivity matrix given as

$$[\mathbf{k}] = \text{diag}[k_1, k_2, k_3] \tag{19}$$

k_1, k_2 and k_3 are thermal conductivities in material principle directions.

An exponentially decaying cohesive constitutive law is used to model cohesive cracking. The traction vector $\mathbf{t}_c$ is defined as

$$\mathbf{t}_c = (1-\omega) f_o \mathbf{r} \tag{20}$$

where $\mathbf{r}$ is a unit vector in the direction of the opening displacement, f_o is the magnitude of peak tractions in the mixed mode. The mode-mixity is taken into account by the Benzeggagh-Kenane mode-mixity criterion [9]. ω is a damage variable which varies from 0, the undamaged state, to 1, the fully damaged state. The damage variable ω, is defined as:

$$\omega = 1 - exp(1) \cdot \left(\frac{[\![u]\!]}{[\![u]\!]_o}\right) \cdot exp\left(-\frac{[\![u]\!]}{[\![u]\!]_o}\right) \tag{21}$$

in which $[\![u]\!]_o$ is the magnitude of displacement jump corresponding to peak traction f_o.

4 Numerical examples

In this section different numerical examples are presented to demonstrate the validity and salient features of the discontinuous thermo-mechanical model.

4.1 Edge crack under constant heat flux

To validate the proposed numerical model, a square unidirectional plate with an edge crack is considered, figure 2a. The fiber orientation is in the direction of y-axis.

The plate is modeled with orthotropic material properties with E_1=25E4MPa, E_2=E_3=1E4MPa, G_{12}=12.5E4MPa, ν_{12}=0.25, ν_{23}=0.25, k_1=1.65E-4W/(mC), k_2=k_3=2.46E-6W/(mC), α_1=-0.3E-6C^{-1}, α_2=α_3=30E-6C^{-1}.

The plate is subjected to a uniform temperature θ_o = -22^{o}C on the top surface, while the temperature at the bottom surface is prescribed as 0^{o}C. The plate is discretized with a finite element mesh of 52x52x1 solid elements.

The exact solution for temperature distribution is given by $\theta = \frac{y}{100}\theta_o$. The numerical result in the form of temperature distribution is presented in figure 2b. The numerical result is in agreement with the exact solution. It is also evident that the presence of a crack did not affect the temperature field.

4.2 Adiabatic cracking

A unidirectional edge cracked plate is analyzed to see the performance of the thermo-mechanical model in simulating mesh-independent adiabatic cracking phenomena. Model geometry and boundary conditions are shown in figure 3a. The material properties and finite element mesh discretization is the same as used in section 4.1. To simulate adiabatic cracking the plate is subjected to a uniform temperature $\theta_o = 22^o$C on the right edge and the temperature at the left edge is 0^oC, figure 3a. Figure 3b shows the temperature distribution for the case in which the fibre direction is parallel to the y-axis. Figure 3c shows the temperature distribution for the case in which the fiber direction is parallel to x-axis. Figures 4a and 4b show the tem-

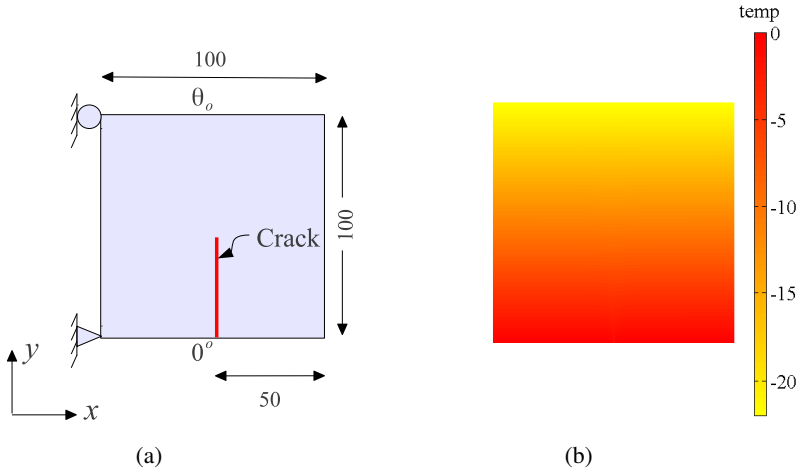

(a) (b)

Fig. 2. Edge crack under constant heat flux, (a) model geometry and boundary conditions (All dimensions in mm), (b) analysis result: temperature distribution

perature distribution on two faces of the crack along the crack line for the two cases. It can be observed from the analysis results that the discontinuity in the temperature field is properly modeled. The difference in temperature field on both sides of the crack is significant for the case in which the fiber orientation is perpendicular to the direction of the crack (figure 3c) compared to the case in which the fiber orientation is parallel to the crack (figure 3b). This is due to a high thermal conductivity in the fiber direction.

To show the capability of the model for inclined cracks, a unidirectional plate with an inclined crack is considered. The geometry and boundary conditions are shown in figure 5a. The fiber direction is at an angle of 105^o with the x-axis. Note that the initial crack is also along the fiber direction. The analysis is performed with the same finite element mesh as used in section 4.1. Figure 5b shows the result of the analysis in the form of a temperature distribution. Figure 6 shows the temperature distribution on two faces of the crack.

4.3 Isothermal cracking

A square unidirectional edge cracked plate is considered to simulate isothermal cracking. The model geometry and boundary conditions are shown in figure 7a. Fiber orientation is parallel to the y-axis. To simulate isothermal cracking, rate of interface dissipation ($\mathbf{t} \cdot [\![\dot{\mathbf{u}}]\!]$) is given as an input in this example. However, it is to note that in real simulations this is not the input. In real simulations this is computed from the mechanical part of the equilibrium. This will be demonstrated in the next section. In this example a constant rate of dissipation (2.0E-5Nmm$^{-1}s^{-1}$) is prescribed along the crack surface.

Figure 7b shows the analysis result in the form of temperature distribution. Temperature distribution on two faces of the crack is shown in figure 8. It is evident from the figure that the discontinuous thermo-mechanical model is also able to simulate a weak discontinuity in the temperature field.

4.4 Edge-notch plate under impact

To demonstrate the capability of the thermo-mechanical model to simulate heat generation during damage growth under impact loading, an edge-notch plate is considered. The geometry and boundary conditions are shown in figure 9a. The plate is modeled with isotropic material properties: E=200.227GPa, ν=0.25, k=15W/(mC), α=1E-5C^{-1}, ρ=7830Kgm^{-3}, C_p=50J/(KgC).

The plate is subjected to two different velocities, v = 1E0mm/s and 1E2mm/s. Integration in the time do-

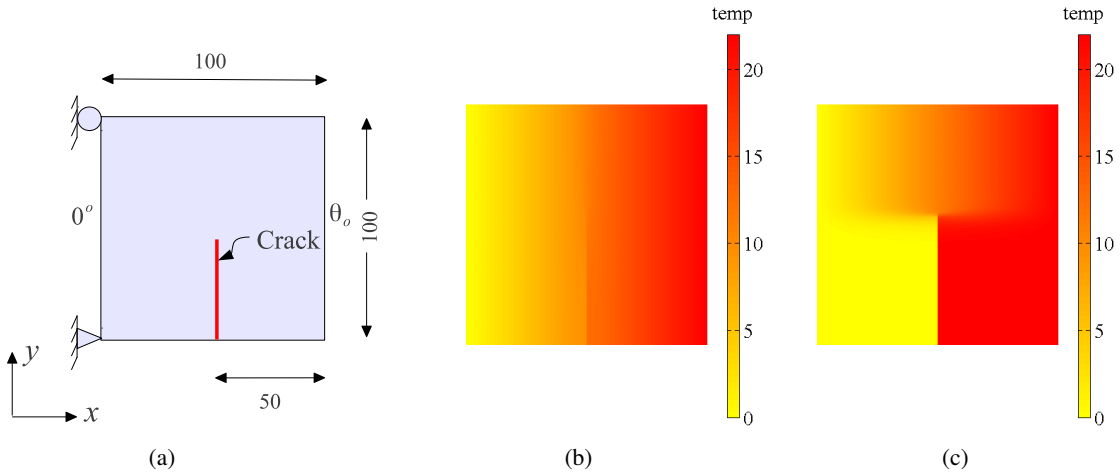

(a) (b) (c)

Fig. 3. Edge crack under adiabatic conditions, (a) model geometry and boundary conditions (All dimensions in mm), (b) temperature distribution in a laminae with fibre orientation along y-axis, (c) temperature distribution in a laminae with fiber orientation along x-axis

main is performed with the Newmark constant average acceleration method.

Figure 9b and 9c show the results of the analyses. The figures depicts the temperature distribution at u = 0.065mm. It can be observed from the figures that a bulb of heat is generated along the crack surface due to dissipative processes during fracture. It can also be observed that with the increase in impact velocity the temperature rise is larger, figure 9c. Moreover, as the impact velocity becomes larger, the heated area becomes smaller. This is due to the fact that at higher rates of loading adiabatic conditions prevail and the effect of heat conduction is negligible over the domain of the plate.

Figure 10 compares the load-displacement curves for two analyses cases. Integrating the area under the curves show that the energy dissipated is 73.7077Nmm for v=1E0mm/s and 74.8159Nmm for v=1E2mm/s. This is in close agreement with the fracture energy multiplied with the width of the plate (excluding the length of the notch), which is 72.7950Nmm. The excess dissipated energy in the numerical results can be attributed to the rate effects due to inertia and thermo-mechanics.

5 Concluding remarks

A discontinuous, coupled thermo-mechanical model for fibre reinforced composite plates is presented. The model is able to simulate mesh-independent discontinuities in the displacement, temperature and heat flux fields. The discontinuity is incorporated using the phantom node method which allows efficient finite element implementation. Numerical results show that the thermo-mechanical model is capable of simulating mesh-independent isothermal and adiabatic cracking in FRP laminates. The model properly takes into account the damage growth under coupled thermo-mechanics. Moreover, the model is also able to capture thermally induced rate effects.

Acknowledgements

Financial support from N-W.F.P University of Engineering & Technology Peshawar, Pakistan, under the HEC approved project titled “Strengthening of existing earthquake engineering center” and Delft University of Technology, Netherlands is gratefully acknowledged.

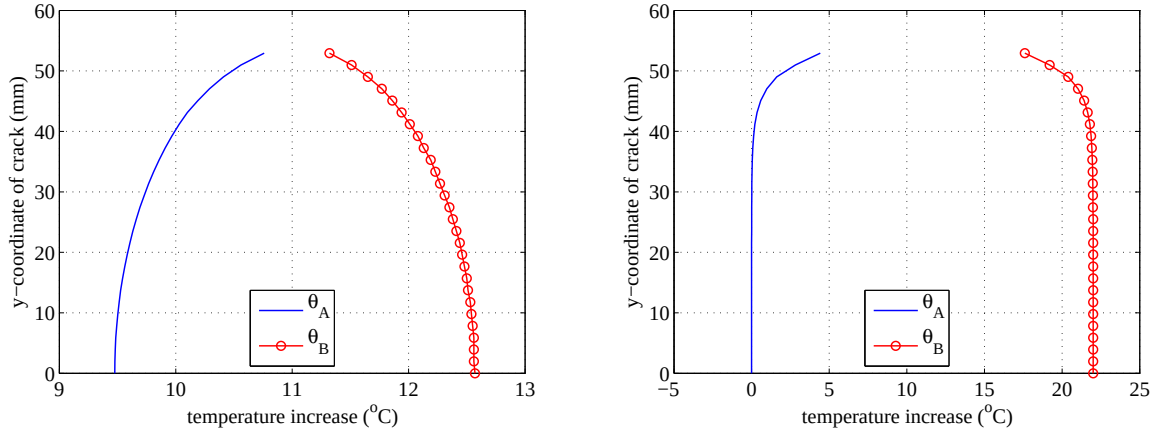

Fig. 4. Temperature distribution on two faces of the crack, (a) temperature distribution with fibre orientation along y-axis, (c) temperature distribution with fiber orientation along x-axis

References

[1] Z. Li, J. Lambros "Dynamic thermo mechanical behavior of fiber reinforced composites". *Composites: Part A*, Vol 31, pp 537-547, 2000.

[2] D. Coker and A.J. Rosaki "Experimental observations of intersonic crack growth in asymmetrically loaded unidirectional composite plates". *Philosophical magazines A*, Vol. 81, No. 3, pp 571-595, 2001.

[2] A.J. Rosaki "Intersonic shear cracks and fault ruptures". *Advances in physics*, Vol. 51, No. 4, pp 1189-1257, 2002.

[4] T.W. Bjerke and J. Lambros "Heating during shearing and opening dominated dynamic fracture of polymers". *Experimental mechanics*, Vol. 42, No. 1, pp 107-114, 2002.

[5] J.M. Melenk and I. Babuska "The partition of unity finite element method: basic theory and applications". *Computer methods in applied mechanics & engineering*, Vol 139, pp 289-314, 1996

[6] J. Mergheim, E. Kuhl and P. Steinmann "A finite element method for the computational modelling of cohesive cracks". *International journal of numerical methods in engineering*, Vol 63, pp 276-289, 2005

[7] M. Fagerstrom and R. Larsson "A thermo-mechanical cohesive zone formulation for ductile fracture". *Journal of mechanics and physics of solids*, Vol. 56, pp 3037-3058, 2008.

[8] A. Hattiangadi and T. Siegmund "A numerical study on interface crack growth under heat flux loading". *International journal of solids and structures*, Vol. 42, pp 6335-6354, 2005.

[9] M.L Benzeggagh and M. Kenane "Measurement of mixed-mode delamination fracture toughness of unidirectional glass/epoxy composites with mixed-mode bending apparatus". *Composites science and technology*, Vol. 56, pp 439-449, 1996.

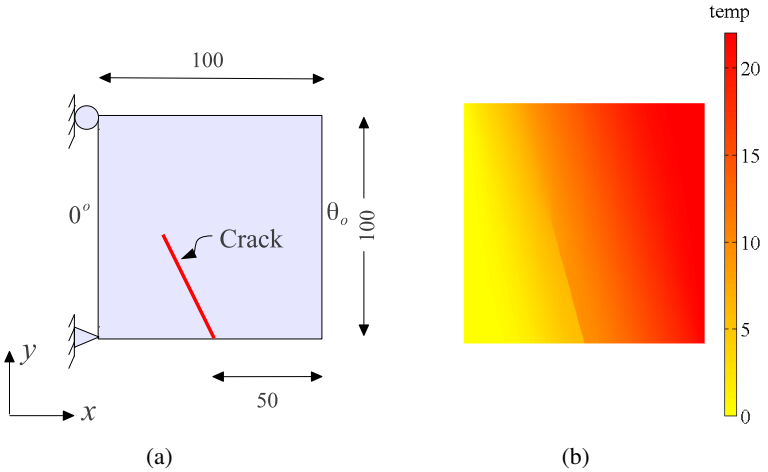

(a) (b)

Fig. 5. Inclined edge crack under adiabatic conditions

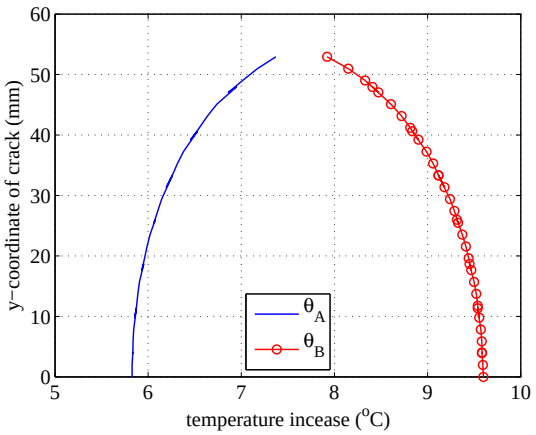

Fig. 6. Temperature distribution on two faces of the crack-Inclined crack

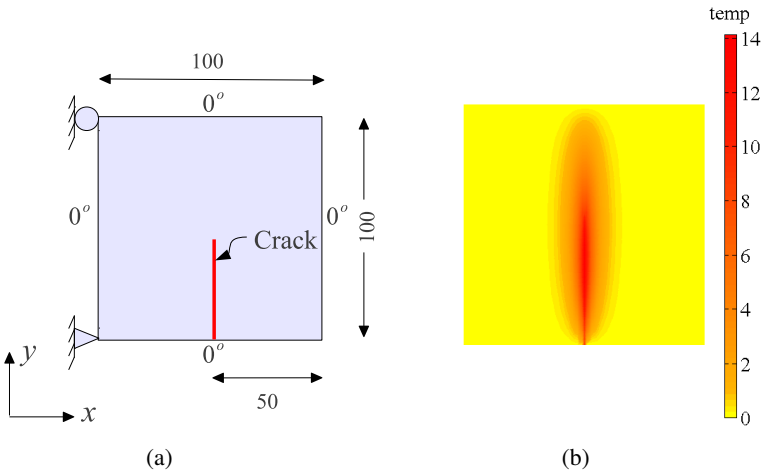

(a) (b)

Fig. 7. Isothermal cracking in a unidirectional laminae

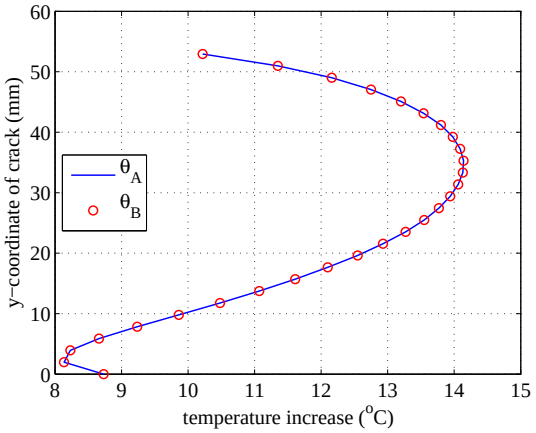

Fig. 8. Temperature distribution on two faces of the crack - Isothermal cracking

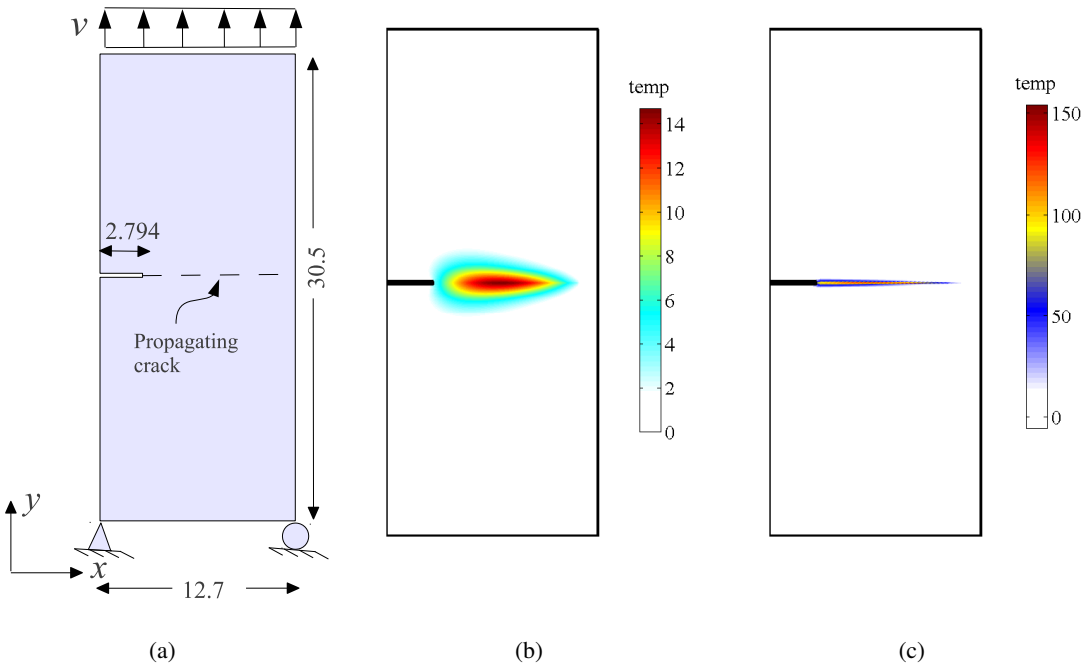

Fig. 9. Edge-notch plate under impact; (a) model geometry and boundary conditions (All dimension in mm), (b) temperature profile for v = 1E0mm/s, (c) temperature profile for v = 1E2mm/s

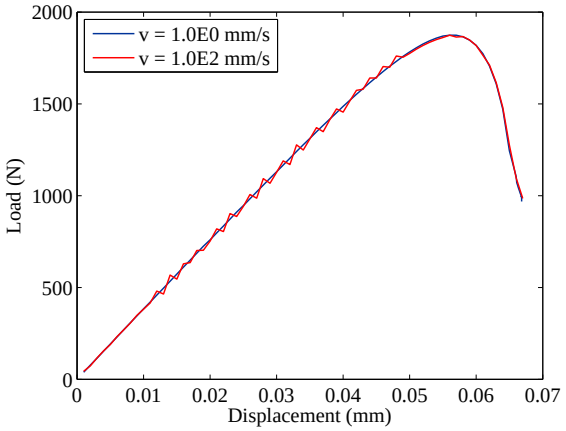

Fig. 10. Load-displacement response of edge-notch plate under impact